Full Text View

Volume 29, Issue 6 (June 1999)

Journal of Physical Oceanography
Article: pp. 1239–1250 | Abstract | PDF (289K)

Adaptive Mesh Refinement for Finite-Difference Ocean Models: First Experiments

Eric Blayo and Laurent Debreu

Projet IDOPT, Laboratoire de Modélisation et Calcul, Université Joseph Fourier, Grenoble, France

(Manuscript received November 13, 1997, in final form July 6, 1998)

DOI: 10.1175/1520-0485(1999)029<1239:AMRFFD>2.0.CO;2

ABSTRACT

The application of an adaptive mesh refinement (AMR) method for structured mesh is examined in the context of ocean modeling. This method can be used with existing finite-difference ocean models at little computational and programming cost. Some first experiments in academic cases are presented in order to give some insight to the two following questions: (i) Is the AMR method appropriate and efficient for integration of numerical ocean circulation models (and particularly for long-term integration)? (ii) Can the AMR method be an efficient alternative to the classical zoom techniques for local prediction?

Numerical simulations are performed in the well-known case of the barotropic modon and in the case of a multilayered quasigeostrophic box model. They demonstrate that the use of the AMR method results in a very significant gain in CPU time (by a factor of 3) while conserving, within a 10%–20% range, the main statistical features of the solution obtained with a uniformly high resolution. For the problem of local prediction, it appears that only one simulation with the AMR method leads to better local predictions than classical nested grid techniques, wherever the region of interest is located, and for a comparable amount of computation. Further investigations are presently under way to generalize this application to basin-scale primitive equation models in realistic configurations and investigate whether or not these results are still valid.

1. Introduction

The problem of spatial resolution is a key point in ocean modeling. Since several numerical experiments demonstrated the

strong interactions of the mesoscale eddy activity with the large-scale circulation (e.g., Holland 1978; Barnier et al. 1991), it seems to be an important condition for numerous oceanic studies to use eddy-resolving ocean general circulation models. In other respects, fine spatial resolution is also of interest to improve the representation of particular local phenomena, for example, due to strong bathymetric gradients or to irregularities of the coastline shape. Moreover, the requests for high-resolution prediction of the ocean circulation in limited areas are presently increasing in conjunction with the development of operational oceanography.

However, given the characteristic scales of ocean circulation (basins of thousands of kilometers, timescales of months to years), the computational cost is, and will still remain in the forthcoming years, a limiting factor for ocean modelers. Any high-resolution basin-scale simulation requires hundreds or thousands of hours of CPU time on present supercomputers. Thus, the interest in numerical methods that could possibly reduce the computational cost of ocean models while still allowing locally high resolution is evident.

The finite element technique allows, of course, the use of a nonuniform resolution over the computational domain. In the field of ocean modeling, this approach has been mostly developed for coastal dynamics (e.g., Lynch and Werner 1987, 1991) and ocean tide models (e.g., Le Provost et al. 1994a, and references therein). The feasibility and utility of finite element methods for modeling the general ocean circulation was first addressed by Fix (1975), who studied the properties of the method (stability, convergence, conservation laws) for a barotropic model. Haidvogel et al. (1980) compared the precision of a finite-difference model, a finite element model, and a spectral model for applications to open ocean problems, while Le Provost et al. (1994b) performed a somewhat similar work for basin-scale quasigeostrophic (QG) dynamics. Le Roux et al. (1998) studied recently the performance of several finite-element basis functions for the discretization of the linear shallow water equations, with the aim of developing a finite-element ocean general circulation model.

However, to our knowledge, no finite element model is used presently for large-scale ocean circulation studies. Most ocean models use structured grids, and local refinement in this context of finite differences is always performed via nested grids, that is, a fixed high-resolution local model embedded in a larger coarse grid model. The interaction between the two components is twofold: the lateral boundary conditions for the fine grid are supplied from the coarse grid solution, while the latter is updated from the fine grid solution in the area covered by both grids. Spall and Holland (1991) and Laugier et al. (1996) applied this approach to the two test problems of a barotropic modon and a baroclinic vortex, while Oey and Chen (1992) performed an application to the Norwegian coastal current. In addition, Fox and Maskell (1995, 1996) investigated the interest of vertical refinement, in particular for the representation of bottom topography, with an application to the Iceland–Faeroe Front. However, this nested grid technique is mainly used as an efficient way to supply open boundary conditions in regional ocean models since no particular attention is paid to the solution in the outer domain.

In the present study, we would like to use a more general approach to the problem of local grid refinement for finite-difference ocean models. It is well known that the ocean circulation presents multiple spatial scales, with complex interactions. From the point of view of numerical modeling, the locations where high resolution is needed are mainly related to the presence of energetic and turbulent structures such as fronts and eddies, while coarser resolution may be sufficient in other areas. However, such structures evolve in time and space. That is why an adaptive resolution could be a way to reduce the computational cost of ocean models while conserving the advantages of high resolution. In this context, the adaptive mesh refinement (AMR) method for structured grids introduced by Berger and Oliger (1984) seems well suited for such an attempt. Moreover, it does not require the development of new models, but can be added to existing ones.

This paper is devoted to the presentation of the AMR method and to the investigation of its potential capabilities for ocean modeling through the description of some numerical tests in academic cases. Experiments with a high-resolution primitive equation model of the North Atlantic are currently under way, and their results will be presented in a second paper. We will focus here on two main questions: (i) Is the AMR method appropriate and efficient for integration of numerical ocean circulation models (and particularly for long-term integration since this method was mostly used to our knowledge for short-term process studies: shock hydrodynamics, turbulent flows, short-term meteorology . . .) and (ii) can the AMR method be an efficient alternative to the classical zoom techniques for local prediction? The present paper is organized as follows: The AMR method is presented in section 2. Its adaptive aspect is illustrated in section 3 in the simple case of a barotropic modon. Then results from high-resolution fully turbulent experiments with a multilayered quasigeostrophic model are presented and discussed in section 4. Finally, some conclusions are drawn in section 5.

2. The AMR method

a. General description

The AMR method was introduced by Berger and Oliger (1984) and Berger and Colella (1989), and a complete description of the method can be found in these papers. Note that this method was successfully tested by Skamarock et al. (1989) and Skamarock and Klemp (1993) in the context of numerical weather prediction. It is designed for the solution of systems of partial differential equations using finite-difference techniques. The basic idea of this method is to attain a given accuracy for

a minimum amount of work. Therefore, estimates of the truncation error are computed, and refined grids are created (or existing ones are removed) where and when necessary. Moreover, this approach is recursive in that fine grids can contain even finer grids. So the AMR strategy features a hierarchy of resolution levels, each of which contains a set of grids (Fig. 1). Every grid is covered by some set of parent (coarser) grids, the root level consisting of one coarse-resolution grid covering the entire domain of computation. The refinement ratio of spatial and temporal resolution between two adjacent levels is a given integer r (typically $r = 2$, 3, or 4). So, if we note Δh_l, and Δt_l, the grid spacing, and the time step on every grid at level l, then

$$\frac{\Delta h_l}{\Delta h_{l+1}} = \frac{\Delta t_l}{\Delta t_{l+1}} = r. \qquad (1)$$

With such a convention, once Δh_0 and Δt_0 are chosen on the root grid, the corresponding CFL criterion is automatically verified for all grids. Note, however, that the grid spacing may of course be different in the spatial directions.

The integration algorithm is summarized in Fig. 2. The integration starts at the root level. The solution on the root grid is advanced one time step Δt_0. Then this solution is interpolated in time and space to provide boundary conditions for the grids at level 1, which can then be advanced r time steps Δt_1 and so on recursively for grids at deeper levels. Since $\Delta t_{l-1} = r\Delta t_l$ for each level l, grids at level l have caught up in physical time with the coarser level $l - 1$ at the end of r fine time steps Δt_l. The solution at level $l - 1$ is then updated using the solution at level l (the update methods and related conservation issues are addressed in a following section).

The initialization of the model can be done in several ways: with a coarse grid only or with one or several fine grids, partially or even fully covering the domain, in order to introduce high-resolution features. The AMR will then transform this initial grid hierarchy into a more adequate one at the first regridding step, following its own internal criteria.

Note that, if the maximum number of grid levels is fixed to two and if the location of the fine grids is imposed (i.e., if the adaptive aspect of the method is inhibited), then the AMR method reduces to the classical nested grid technique.

Finally, it must also be pointed out that we have implemented this method in such a way that the ocean model is seen as a black box; almost no modifications to the original code are required. Moreover the management of the grids, the computation of the error estimate, and the refinement procedure involve only a marginal computational cost, mostly because meshes are resized and relocated only every N time steps Δt_0. This package will be made available to the scientific community.

b. Refinement procedure

As mentioned previously, the grid hierarchy may change from one coarse time step to the other. In practical applications, estimates of the truncation error are computed at regular intervals (every N coarse time steps) and grid points are detected where a finer grid is necessary or where an existing fine grid is no longer useful. The estimation is performed with Richardson's method. Let $L_{\Delta h}$ be a finite-difference operator that advances the numerical solution from one time step Δt on a uniform mesh of spacing Δh. If we assume that the spatial and temporal truncation errors are of the same order (this is usually the case in ocean models, which mostly use second-order temporal and spatial schemes), then we have

$$u(x,\ t\ +\ \Delta t) = L_{\Delta h}u(x,\ t)\ +\ (\Delta h)^{q+1}f(x,\ t) + (\Delta t)^{q+1}g(x,t) + O(\Delta h^{q+2}, \Delta t^{q+2}), \qquad (2)$$

where u is a smooth enough solution of the PDE. If two time steps are performed, we obtain

$$u(x, t + 2\Delta t) = L^2_{\Delta h}u(x,\ t)\ +\ 2(\Delta h)^{q+1}f(x,\ t) + 2(\Delta t)^{q+1}g(x,t) + O(\Delta h^{q+2}, \Delta t^{q+2}). \qquad (3)$$

One can also use the same difference operator with a time and space grid of size $2\Delta t$ and $2\Delta h$. This leads to

$$+ (2\Delta t)^{q+1} g(x, t) + O(\Delta h^{q+2}, \Delta t^{q+2}). \quad (4)$$

Subtracting these two last equations leads to the following estimate of the local truncation error:

$$(\Delta h)^{q+1} f(x, t) + (\Delta t)^{q+1} g(x, t) = \frac{L^2_{\Delta h} u(x, t) - L_{2\Delta h} u(x, t)}{2^{q+1} - 2} + O(\Delta h^{q+2}, \Delta t^{q+2}). \quad (5)$$

Such an estimation procedure can be easily implemented on every level of the grid hierarchy. One has to coarsen the data on a given grid by a factor of 2. Then advance this coarsened solution one coarsened time step and compare the result with the current solution advanced two time steps using the preceding formula. If the truncation error is too large, then the grid point is flagged to indicate that a finer grid must be created there. Note that similar criteria can of course also be derived when the spatial and temporal truncation errors are of different orders, or even if they are unknown (Marchuk and Shaydourov 1983). In addition to this purely mathematical criterion, one can also use physically meaningful constraints to ask for refinement when local quantities (e.g., potential vorticity or kinetic energy) are higher than a prescribed value.

The grid points requiring the same level of resolution are then clustered into rectangular subgrids, as can be seen in Fig. 1. An efficient regridding procedure is described, for example, in Berger and Rigoutsos (1991).

c. Updating the solution

We pointed out in the general description of the method that if a level l is not the finest one in the grid hierarchy, the solution on the grids at level l is updated after each time step Δt_l using the solution on the finer grids at level $l + 1$. This update can be performed in several ways, the usual ones being either an average of neighboring fine grid values or even a simple copy of the fine grid values at corresponding coarse nodes.

However, additional numerical schemes can also be used to ensure flux conservation of the model variables at the interfaces between those coarse cells that are overlapped by fine cells and those that are not. Kurihara et al. (1979) proposed a simple methodology for this correction. Let I be the interface between a fine grid at level $l + 1$ and a coarser grid at level l. Fluxes through I can be computed from the fine grid solution and summed over all the r fine time steps Δt_{l+1} that constitute a coarser time step Δt_l. This gives a so-called fine flux. The corresponding "coarse flux" through I is also computed, using the coarse solution only. Then the difference between the fine fluxes and the coarse fluxes is uniformly distributed to correct the coarse values along the interfaces in order to ensure conservation.

Other methods have also been developed recently in nested grid applications. Laugier et al. (1996) make the solution fluxes satisfy a weak continuity relation over a control volume via an iterative method; Perkins et al. (1997) propose a "near continuity" of prognostic model variables performed through a radiation of the difference between inner and outer solutions.

All these strategies can, of course, be applied in the context of the AMR method. However, it must be noted that the problem of flux conservation is intrinsically less crucial with the AMR than with classical nested grid calculations. As a matter of fact, AMR places automatically the fine-to-coarse interfaces where fine grids become no longer useful, that is, where coarse and fine solutions are not very different, which is obviously not the case when the grids are fixed.

3. A simple illustration: The barotropic modon

The AMR method and its ability to refine the model grid where and when necessary will be first illustrated in the well-known case of the barotropic modon. This structure corresponds to a solution of the barotropic vorticity equation in the beta-plane approximation, without wind and dissipation,

$$\frac{\partial \xi}{\partial t} + J(\psi, \xi) + \beta \frac{\partial \psi}{\partial x} = 0, \quad (6)$$

where ψ is the barotropic streamfunction, ξ is the relative vorticity, J is the Jacobian operator, and β is the meridional gradient of the Coriolis parameter at the midlatitude of the domain. An analytic solution was found by Flierl et al. (1980). Its expression in polar coordinates (r, θ) is

$$\psi(r,\theta)=\begin{cases}\left[k^2J_1(k)\left(1+\frac{1}{k^2}\right)a\right]\psi_0\sin\theta, & 0\le r\le a\\ -\left(\frac{K_1(r/a)}{K_1(1)}\right)\psi_0\sin\theta, & r>a,\end{cases}$$

where a is the radius of the modon and J_1 and K_1 are Bessel functions. This modon will propagate eastward at a uniform speed C. Choosing $C=\beta a^2$ imposes the value of the wavenumber $k=3.9226$ (Flierl et al. 1980).

As mentioned previously, the barotropic modon was chosen by Spall and Holland (1991) and Laugier et al. (1996) for numerical tests of nested grid procedures. We have chosen here parameter values similar to those previous studies in order to compare the numerical results. The radius of the modon a is taken equal to 75 km, and $\beta=1.78\times10^{-11}$ m^{-1} s^{-1}, which corresponds to a latitude of 38.5°N. The eastward velocity of the modon is thus 0.1 m s^{-1}. The computational domain is 750×750 km^2. The AMR method is used in this simple case with only two levels of grids with a grid ratio of 4. The coarse-grid spacing is $\Delta h_0=15$ km with a timestep $\Delta t_0=8$ h, while the fine grid parameters are $\Delta h_1=3.75$ km and $\Delta t_1=2$ h. The truncation error is estimated every 10 coarse time steps, and a regridding is then performed if necessary. Initially, the modon is located at the center of the domain in a fine grid of 300×300 km^2. As can be seen in Fig. 3b, this fine grid propagates eastward with the modon, which is not the case in classical nested grid calculations (Fig. 3a).

The results from the AMR calculations are compared with results from a coarse grid computation (uniform mesh size Δh_0), a fine grid computation (uniform mesh size Δh_1), and a nested grid (NG) computation similar to those performed by Spall and Holland (1991) and Laugier et al. (1996). The error with regard to the exact analytical solution is computed, and its integrated value is plotted as a function of time in Fig. 4a. As could be anticipated, the AMR and the NG calculations perform rather similarly as far as the modon remains in the nested domain (approximately until day 9), but the AMR leads to much better results as soon as the modon significantly departs from the center of the domain. At the end of the simulation (day 29), the rms error is equal to 34% in the NG run, but only to 14% in the AMR run. Also of importance is that this improvement is achieved for a low additional cost: the AMR run requires 15.5 s CPU time while the NG run requires 14.1 s (see Table 1).

Another important issue is the efficiency of the AMR for local prediction. This point is illustrated in Fig. 4b. As in Fig. 4a, we computed the evolution with time of the rms error, but integrated only over the central inner domain, which is supposed to be of particular interest. This domain corresponds to the fixed fine grid in the NG calculation and to the initial location of the fine grid in the AMR run, but one must notice that this domain is no more refined after some days in the AMR run. However, the AMR method leads to better results than the NG method, even in this area. As a matter of fact, the rms error is equal to 14% on day 20 and 45% on day 29 in the NG run, but decreases to 7% and 20%, respectively, in the AMR run. This illustrates that increasing the local resolution is not necessarily the best way to improve a result in an area of particular interest. It can be more fruitful to increase the resolution in some critical areas, even out of the area of interest, in order to reduce more efficiently the local numerical error. This point will be further discussed in the following section, but AMR already appears as a possible efficient alternative to classical zoom techniques.

4. Experiments with a multilayered QG model

We will now describe an application of the AMR method in the context of a multilayered QG box model. Such a model is known as a simple prototype of eddy-active large-scale circulation in the midlatitudes. A number of papers can be found dealing with such models in the literature (e.g., Holland 1978; Schmitz and Holland 1982), and the interested reader can refer to these for further details.

The vertical stratification of the ocean is approximated by dividing the total depth into N layers, each layer k being of constant density ρ_k. The reduced gravity at the interface between layers k and $k+1$ is defined by $g'_{k+1/2}=g(\rho_{k+1}-\rho_k)/\rho_0$, g being the acceleration due to gravity and ρ_0 a reference density. The thickness at rest of layer k is denoted by H_k. The classical beta-plane approximation is used, so the Coriolis parameter f is written $f(y)\approx f(y_0)+\beta(y-y_0)$, where y_0 corresponds to the midlatitude of the domain, and

$$\beta=\frac{df}{dy}(y_0).$$

The governing equations can be written as

$$\frac{D}{Dt}\left[\Delta\psi_k + f + \frac{f_0}{H_k}(h_{k+1/2} - h_{k-1/2})\right] = F_k + D_k,$$

$$k = 1, \ldots, N,$$

where D/Dt is the Lagrangian operator $\partial/\partial t + J(\psi, \cdot)$. The variables are the streamfunction ψ_k and the vorticity $\xi_k = \Delta\psi_k$ in each layer. Here $f_0 = f(y_0)$ is the Coriolis parameter at the midlatitude of the domain, and $h_{k+1/2}$ is the height of the interface perturbation. It can be expressed as $f_0(\psi_{k+1} - \psi_k)/g'_{k+1/2}$, $(k = 1, \cdots, N-1)$, with $h_{1/2} = 0$ (rigid-lid approximation) and $h_{N+1/2} = 0$ (flat bottom). The term F_k expresses the influence of the wind on the upper layer:

$$F_1 = \frac{1}{\rho_0 H_1}\,\mathrm{curl}\,\boldsymbol{\tau},$$

where τ is the horizontal wind stress at the surface of the ocean and $F_k = 0$ for any $k > 1$. The dissipation of subgrid-scale processes is ensured by the use of a biharmonic lateral viscosity operator: $D_k = A_4\nabla^4\xi_k$ $(k = 1, \cdots, N-1)$. In the bottom layer, another dissipative term is added to take into account bottom friction:$D_N = A_4\nabla^4\xi_N - C_b\xi_N$.

We choose a configuration similar to an experiment by Barnier et al. (1991), which results in an intense eastward jet associated with a strong eddy activity (Fig. 5). The model is six-layered, with depths of 300, 350, 400, 500, 1350, and 2100 m. The basin has horizontal dimensions of 3600 km × 3200 km. The stratification parameters are fairly standard and lead to Rossby radii of deformation of 38.8, 18.7, 12.6, 10.2, and 9.2 km, respectively. The rotation parameters are $f_0 = 9.3 \times 10^{-5}$ s^{-1} and $\beta = 2 \times 10^{-11}$ m^{-1} s^{-1}. The wind-stress curl forcing is sinusoidal with an amplitude $\tau_0 = 6 \times 10^{-5}$ m^2 s^{-2}. The bottom friction coefficient is $C_b = 10^{-7}$ s^{-1}.

a. Efficiency of the AMR for long-term integration

A spinup of the model was performed with a uniform 10-km horizontal resolution and a lateral friction coefficient $A_4 = 0.25 \times 10^{10}$ m^4 s^{-1}. This simulation was 10 years long in order to reach a statistically steady state. Then the model solution at the end of this run was taken as the initial condition for three experiments. In each case, the model was run for a sequence of 5 years, and flow statistics were computed and compared to assess the effectiveness of the AMR method for long-term integrations. Experiment G-10 was performed with an uniform 10-km horizontal resolution in both directions, and a lateral friction coefficient $A_4 = 0.25 \times 10^{10}$ m^4 s^{-1}; experiment G-40 with 40-km resolution and $A_4 = 64 \times 10^{10}$ m^4 s^{-1} (these values of A_4 ensure consistency between the dissipation timescales on the different grids). A third experiment G-AD was performed using AMR with a grid ratio $r = 4$ and two levels of grids corresponding to G-40 and G-10. The refinement criterion is that the error estimate of the velocity in the upper layer must be less than 2 cm s^{-1}. The interpolation from the coarse grid to the fine grids is performed with cubic splines for the initialization of the fine grids and with Lagrange polynomials for the specification of the boundary conditions. The coarse grid values are updated by a simple copy of the corresponding fine grid values. Conservation of mass between coarse and fine meshes is implicitely ensured by these procedures since the model variable is the streamfunction. On another hand, strict conservation of energy is not imposed since this is not appropriate on a nested mesh (Kurihara et al. 1979; Peggion 1994).

Examples of instantaneous surface circulation corresponding to these simulations are displayed in Fig. 5. Since the mesoscale activity is not properly resolved with the 40-km resolution, the level of instability is much weaker in experiment G-40 than in experiment G-10, and the transfer of energy from the eddy flow to the mean flow is not sufficient to lead to the formation of an intense central jet. However, as can be seen in Fig. 5c, the adaptive method working with a 40-km coarse grid plus a 10-km fine grid where and when necessary seems able to reproduce the eddy activity of the flow observed in the 10-km case. An important point here is, of course, the computational cost of the G-AD simulation, which is three times lower than the cost of the G-10 experiment. This is illustrated in Fig. 6, where the mean location of the fine grid in the G-AD experiment is plotted. As can be seen, this fine grid covers on average only about one-third of the domain, corresponding to the areas of maximum eddy energy (see Fig. 8).

We cannot, of course, expect experiment G-AD to give exactly the same results as experiment G-10. The main question here is rather to determine if the solution provided by the adaptive method is acceptable from an oceanographic point of view and if its discrepancies with regard to an uniformly high-resolution experiment are balanced by the gain in CPU time. To try to answer this question, we computed for each experiment some statistics over the 5-yr period. They confirm the reasonable performance of the AMR method in reproducing the main statistical features observed in the G-10 case. The global pattern of the mean circulation is rather similar in the G-AD and G-10 simulations, with a strong central jet penetrating far eastward and its associated northern and southern recirculation cells (Fig. 7). The transports are almost identical in both experiments. However, the penetration length of the jet is reduced by about 10% in the adaptive case. Moreover, the deep inertial cells present in the deep layer of the G-10 experiment in the northwest and southwest corners of the domain are very weakened in G-AD, by a factor of almost 2. This is explained by the fact that the refinement criterion used in these simulations deals only with the solution in the upper layer, which does not present an important activity in these regions. A generalized criterion using information from every layer would probably solve this problem, but we think that the derivation of such a criterion is out of the scope of this study with this nonrealistic model. However, we will have to formulate such generalized criteria when using realistic models.

The mean levels of kinetic energy in each layer are displayed in Table 2. As can be seen, the adaptive method leads to similar values as in the 10-km case, within a range of roughly 10%. This is also the case for the eddy activity. The spatial distribution of eddy kinetic energy (Fig. 8) is rather correctly reproduced with the AMR method, with a discrepancy of typically 10%–20% in the numerical values. We have also examined several other diagnostic variables such as sea surface height variability, barotropic and baroclinic structures, and Rossby waves features, which confirm the preceding statement that the AMR method leads to the same flow statistics as the G-10 experiment, within a 10%–20% range.

b. Interest of the AMR for local zooms

Apart from the problem of long-term integration, the other question we want to address in this study is the interest of the AMR method for local prediction, compared to classical nested grid techniques. The barotropic modon experiment presented above suggested that AMR could appear as an efficient alternative to these standard methods. To try to confirm this point, we conducted nested grid experiments in this multilayered QG model framework. Note that we did not choose here a 40-km coarse grid because, as seen previously, it results in dynamics that is very different from the 10-km case. Therefore, nested grid experiments with a 40-km coarse grid cannot lead to correct results, which would bias the comparison with adaptive simulations. That is why we used a 20-km resolution, which leads to a circulation pattern much more similar to the 10-km case than a 40-km grid does.

Two experiments were conducted. In each case, a 10-km inner grid was located over a region supposed to be of particular interest and coupled with a 20-km resolution model covering the whole basin. As can be seen in Fig. 6, the two regions of interest were chosen aside from the mean location of the fine grids in the adaptive simulation. So the major part of the fine grids in the AMR simulation will, in general, be located outside those two regions. The area of each region is equal to 30% of the area of the global domain, which represents also the mean area covered by the fine grids in the adaptive experiment. This was chosen in such a way that the computational costs of each nested grid experiment and of the adaptive experiment would be equal. For each case, the simulation was initialized with a solution obtained with a uniform 10-km resolution model (experiment G-10 above). Then the nested grid model was integrated over a 30-day period, and the rms difference between the reference solution G-10 and the nested grid solution was computed in each layer over the inner domain. These results were then compared with those obtained over the same time period by an AMR simulation, working with two levels of grid (20 and 10 km) and initialized with the same reference solution. These rms differences are displayed in Fig. 9 for the upper layer of the model, but the behavior remains similar for deeper layers. For the first area of interest (area A in Fig. 6, located along the southern boundary), the rms difference at the end of the 30-day period is equal to 6.3% in the 20-km case, 4.5% in the nested grid case, and 3.5% in the adaptive case. Since the circulation and the eddy activity in this region are weak, the coarse-mesh model itself reproduces quite well the circulation obtained with the fine-mesh model. However, the nested grid approach decreases the rms difference by about 30%, and the adaptive case performs even better. The second area of interest (area B in Fig. 6) is located in the eastern part of the domain, downstream from the central jet, and corresponds to a circulation more active than in the previous case. The results are then more spectacular. As a matter of fact, the rms difference at the end of the 30-day period is equal to 19.5% in the 20-km case, 15% in the nested grid case, and only 4.5% in the adaptive case. The interest of the adaptive approach for local prediction is thus particularly striking in this case. Once again, it seems better to increase the resolution in some critical areas, even out of the area of interest, to reduce more efficiently the local numerical error. It is also important to note here that only one AMR simulation is required (which represents the same computation effort as one NG calculation) to provide a solution comparable or better than NG solutions everywhere in the domain.

5. Summary and conclusions

We have presented in this paper some preliminary applications to numerical ocean circulation models of the adaptive mesh refinement method developed by Berger and Oliger (1984). Since most ocean general circulation models use a finite-difference discretization of the equations, we were interested in testing whether or not this method could add interesting

potentialities to existing numerical models. Hence, we developed a Fortran-90 package in which the model is seen as a black box, and which allows adaptive refinement at little computational cost and without programming effort. The adaptivity can, of course, also be inhibited, to perform classical nested grid calculations. Since the concept of the AMR is model independent, it can also be combined with other means to improve numerical simulations, such as high-order methods or subgrid-scale parameterizations.

In the present study, we addressed the behavior of this method in the well-known case of the barotropic modon (already addressed by other authors with nested grid techniques) and in the case of a multilayered QG box model. From the point of view of long-term integration of numerical models, the AMR method proved in the above experiments to allow a significant gain in CPU time (by a factor of 3) while conserving the main statistical features of the uniformly high resolution solution, within a 10%–20% range. Such a method may thus be of interest for the spinup phase of models, or also for applications requiring the computation of approximated statistical properties (this is the case, e.g., of many data assimilation methods derived from filtering theory). The results are also interesting concerning the capabilities of the AMR method for local prediction. It appears in our numerical experiments that a simulation using the AMR method leads to better local predictions than classical nested grid techniques, wherever the region of interest is located.

Even if the present study is deliberately restricted to academic cases, it seems to us that its conclusions are encouraging and justify further investigations. However, the generalization of these results to realistic numerical models of the ocean circulation is, of course, far from being straightforward. The processes involved by a more complete physics and realistic coastlines, bathymetry, and forcings are much more complicated than those encountered in the present numerical simulations. Hence several aspects of the method will require particular attention. For example, the definition of the rules for refinement will be more complex. The problem of vertical refinement will become of interest in relation with topographic effects or representation of particular water masses. It will also be interesting to observe the behavior of the grids: Does the AMR perform a kind of monitoring of ocean energetic and turbulent structures (fronts, eddies, . . .) or are the grids rather static, covering well-known important regions (western boundaries . . .)? That is why we are presently implementing this method in a primitive equation model of the North Atlantic to address these questions and to form a better judgment on the interest of the AMR for ocean modeling.

Acknowledgments

The calculations were made possible by the computer facilities at the Institut du Développement et des Ressources en Informatique Scientifique (IDRIS-CNRS) at the Centre Grenoblois de Calcul Vectoriel (CGCV-CEA). IDOPT is a joint CNRS/University of Grenoble/Institut National Polytechnique de Grenoble/INRIA project.

REFERENCES

Barnier, B., B. L. Hua, and C. Le Provost, 1991: On the catalytic role of high baroclinic modes in eddy-driven large-scale circulations. *J. Phys. Oceanogr.*, **21,** 976–997.. Find this article online

Berger, M., and J. Oliger, 1984: Adaptive mesh refinement for hyperbolic partial differential equations. *J. Comput. Phys.*, **53,** 484–512..

— ,and P. Colella, 1989: Local adaptive mesh refinement for shock hydrodynamics. *J. Comput. Phys.*, **82,** 64–84..

— ,and I. Rigoutsos, 1991: An algorithm for point clustering and grid generation. *IEEE Trans. Systems Man Cybernetics*, **21,** 1278–1286..

Fix, G. J., 1975: Finite element models for ocean circulation problems. *SIAM J. Appl. Math.*, **29,** 371–387..

Flierl, G. R., V. D. Larichev, J. C. McWilliams, and G. M. Reznik, 1980: The dynamics of baroclinic and barotropic solitary eddies. *Dyn. Atmos. Oceans*, **5,** 1–41..

Fox, A. D., and S. J, Maskell, 1995: Two-way interactive nesting of primitive equation ocean models with topography. *J. Phys. Oceanogr.*, **25,** 2977–2996.. Find this article online

— ,and — ,1996: A nested primitive equation model of the Iceland–Faeroe front. *J. Geophys. Res.*, **101,** 18 259–18 278..

Haidvogel, D. B., A. R. Robinson, and E. F. Schulman, 1980: The accuracy, efficiency and stability of three numerical models with application to open ocean problems. *J. Comput. Phys.*, **34,** 1–53..

Holland, W. R., 1978: The role of mesoscale eddies in the general circulation of the ocean. Numerical experiments using a wind-driven quasi-geostrophic model. *J. Phys. Oceanogr.*, **8,** 363–392.. Find this article online

Kurihara, Y. G., G. J. Tripoli, and M. A. Bender, 1979: Design of a movable nested-mesh primitive equation model. *Mon. Wea. Rev.*, **107,** 239–249.. Find this article online

Laugier, M., P. Angot, and L. Mortier, 1996: Nested grid methods for an ocean model: A comparative study. *Int. J. Num. Meth. Fluids*, **23,** 1163–1195..

Le Provost, C., M. L. Genco, F. Lyard, P. Vincent, and P. Canceil, 1994a: Spectroscopy of the world ocean tides from a finite element hydrodynamic model. *J. Geophys. Res.*, **99,** 24 777–24 797..

— , C. Bernier, and E. Blayo, 1994b: An intercomparison of two numerical methods for integrating a quasi-geostrophic multilayer model of ocean circulations: Finite element and finite difference methods. *J. Comput Phys.*, **110,** 341–359..

Le Roux, D. Y., A. Staniforth, and C. A. Lin, 1998: Finite elements for shallow-water equation ocean models. *Mon. Wea. Rev.*, **126,** 1931–1951.. Find this article online

Lynch, D. R., and F. E. Werner, 1987: Three-dimensional hydrodynamics on finite elements. Part I: Linearized harmonic model. *Int. J. Num. Meth. Fluids*, **7,** 871–909..

— , and — , 1991: Three-dimensional hydrodynamics on finite elements. Part II: Nonlinear time-stepping model. *Int. J. Num. Meth. Fluids*, **12,** 507–533..

Marchuk, G., and V. Shaydourov, 1983: *Difference Methods and Their Extrapolations.* Springer, 364 pp..

Oey, L.-Y., and P. Chen, 1992: A nested grid ocean model with application to the simulation of meanders and eddies in the Norwegian coastal current. *J. Geophys. Res.*, **97,** 20 063–20 086..

Peggion, G., 1994: Numerical inaccuracies across the interface of a nested grid. *Numerical Meth. Part. Diff. Eq.*, **10,** 455–473..

Perkins, A. L., L. F. Smedstad, D. W. Blake, G. W. Heburn, and A. J. Wallcraft, 1997: A new nested boundary condition for a primitive equation ocean model. *J. Geophys. Res.*, **102,** 3483–3500..

Schmitz, W. J., and W. R. Holland, 1982: A preliminary comparison of selected numerical eddy-resolving general circulation experiments with observations. *J. Mar. Res.*, **40,** 75–117..

Skamarock, W. C., and J. B. Klemp, 1993: Adaptive grid refinement for 2D and 3D nonhydrostatic atmospheric flows. *Mon. Wea. Rev.*, **121,** 788–804.. Find this article online

— , J. Oliger, and R. L. Street, 1989: Adaptive grid refinement for numerical weather prediction. *J. Comput. Phys.*, **80,** 27–60..

Spall, M. A., and W. R. Holland, 1991: A nested primitive equation model for oceanic applications. *J. Phys. Oceanogr.*, **21,** 205–220.. Find this article online

---

Tables

Table 1. CPU time (in seconds) for the different experiments.

Coarse grid	0.95
Nested grid	14.10
AMR	15.54
Fine grid	54.58

Click on thumbnail for full-sized image.

Table 2. Mean kinetic energy in each layer for each experiment (unit: $cm^2\ s^{-2}$).

Layer	G-10	G-40	G-AD
1	318	137	307
2	125	52	118
3	67	24	58
4	47	15	38
5	39	11	30
6	38	11	29

Click on thumbnail for full-sized image.

Figures

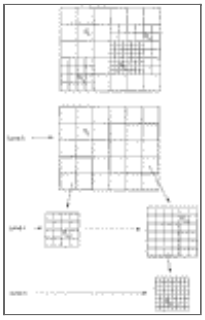

Click on thumbnail for full-sized image.

Fig. 1. An example of grid hierarchy.

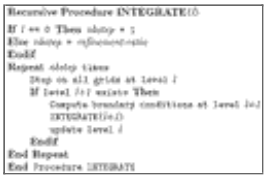

Click on thumbnail for full-sized image.

Fig. 2. Integration algorithm of the AMR method.

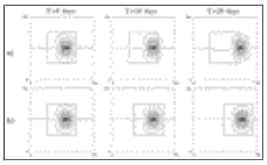

Click on thumbnail for full-sized image.

Fig. 3. Numerical solution of the modon problem at three different time steps (CI: 1000 m^2 s^{-1}) for the (a) nested-grid calculation and (b) AMR calculation. The location of the fine grid is indicated.

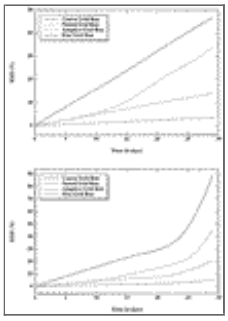

Click on thumbnail for full-sized image.

Fig. 4. Evolution with time of the rms error for the different numerical simulations. Upper panel: rms computed over the whole domain; lower panel: rms computed over the central inner domain only.

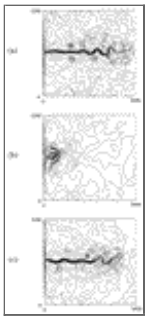

Click on thumbnail for full-sized image.

Fig. 5. Snapshots of the surface circulation for the three experiments: (a) 10-km experiment, (b) 40-km experiment, and (c) adaptive experiment. (CI: 10 000 m^2 s^{-1}.)

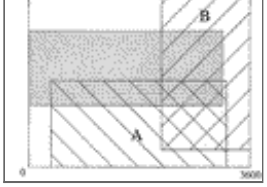

Click on thumbnail for full-sized image.

Fig. 6. Shaded: mean location of the fine grid in experiment G-AD. Labeled: locations of the two zoom areas for the nested grid experiments.

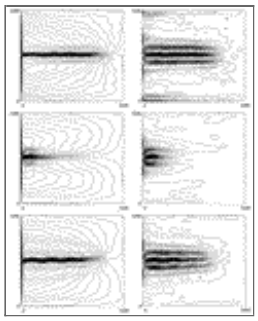

Click on thumbnail for full-sized image.

Fig. 7. Mean circulation in the surface layer (left) and in the bottom layer (right) for the three experiments:(top) 10-km experiment, (middle) 40-km experiment, and (bottom) adaptive experiment. [CI: 5000 m^2 s^{-1} (left) and 1000 m^2 s^{-1} (right).]

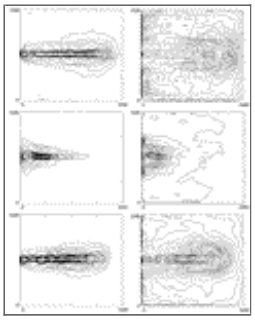

Click on thumbnail for full-sized image.

Fig. 8. Eddy kinetic energy in the surface layer (left) and in the bottom layer (right) for the three experiments:(top) 10-km experiment, (middle) 40-km experiment, and (bottom) adaptive experiment. [CI: 100 cm^2 s^{-2} (left) and 5 cm^2 s^{-2} (right).]

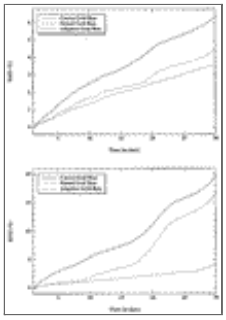

Click on thumbnail for full-sized image.

Fig. 9. Evolution with time of the rms difference with regard to the fine grid reference experiment, for the coarse grid, nested grid, and adaptive experiments. The rms is computed in the surface layer over the area of interest. Upper panel: area A (south); lower panel: area B (east).

Corresponding author address: Dr. Eric Blayo, Laboratoire de Modélisation et de Calcul, Institut de Mathematiques Appliquées de Grenoble, BP 53, 38041 Grenoble Cedex 9, France.

E-mail: Eric.Blayo@imag.fr

top

Headquarters: 45 Beacon Street Boston, MA 02108-3693
DC Office: 1120 G Street, NW, Suite 800 Washington DC, 20005-3826
amsinfo@ametsoc.org Phone: 617-227-2425 Fax: 617-742-8718
Allen Press, Inc. assists in the online publication of *AMS* journals.